Integration Stability Analysis Of Nonlinear Model Predictive Motion Control For Autonomous Vehicles

Linhe Ge
Jilin University State Key Laboratory of Automotive Simulation and Control
Yang Zhao (yang_zhao@jlu.edu.cn)
Jilin University State Key Laboratory of Automotive Simulation and Control https://orcid.org/0000-0003-2338-5671
Shouren Zhong
Jilin University State Key Laboratory of Automotive Simulation and Control
Zitong Shan
Jilin University State Key Laboratory of Automotive Simulation and Control
Fangwu Ma
Jilin University State Key Laboratory of Automotive Simulation and Control
Zhiwu Han
Jilin University State Key Laboratory of Automotive Simulation and Control
Konghui Guo
Jilin University State Key Laboratory of Automotive Simulation and Control

Research Article

Keywords: Motion control, Path tracking, Nonlinear offset free MPC, Integration stability, Runge-Kutta-Chebyshev solver

Posted Date: March 10th, 2022

DOI: https://doi.org/10.21203/rs.3.rs-1391849/v1

Integration Stability Analysis of Nonlinear Model Predictive Motion Control for Autonomous Vehicles

Linhe Ge[1], Yang Zhao[1*], Shouren Zhong[1], Zitong Shan[1], Fangwu Ma[1], Zhiwu Han[1] and Konghui Guo[1]

[1*]the State Key Laboratory of Automotive Simulation and Control, Jilin University, Renmin Street No. 5988, Changchun, 130022, Jilin Province, China.

*Corresponding author(s). E-mail(s): yang_zhao@jlu.edu.cn;

Abstract

There has been a growing interest in nonlinear model predictive control (NMPC) for the motion control of autonomous driving. However, it is odd that integration stability has not been considered enough when developing these applications for autonomous driving. The stabilized explicit Runge-Kutta (RK) integration method is proposed in this paper to solve the integration stability problem in motion control of autonomous vehicles (AVs). In comparison with other explicit integration methods, this method provides a wider stable region and is more efficient than implicit integration methods. This integration method is integrated into the framework of offset free nonlinear MPC solver based on GRAMPC by us. As a result, the problem of computational stability at low speeds of motion control can be resolved. At the same time, a larger integration step size can be adopted, and nonlinear MPC becomes more computationally efficient. The results of simulation and real vehicle experiment results show that the problem of low-speed integration stability when using non-linear dynamic model as a prediction model is successfully solved, which has been ignored in many previous studies.

Keywords: Motion control, Path tracking, Nonlinear offset free MPC, Integration stability, Runge-Kutta-Chebyshev solver

1 Introduction

NMPC is more and more widely used in vehicle stability and motion control because it can accurately predict the state and constraints of the nonlinear system in the future. Both direct and indirect NMPC methods [1] involve the discretization of continuous systems. In fact, the vehicle dynamics system is a relatively fast-changing system, which requires that the discrete-time step size should not be too large. The stability control, especially the path following control, needs a long prediction time horizon. These two reasons lead to the increase of the dimension of the optimization problem and the computational burden. How to use a more stable and accurate discretization method is particularly important to reduce the number of optimization variables and computational burden.

The essence of discretization is actually the process of integration. In other words, all the integration methods of ordinary differential equations (ODE) are suitable for the discretization of system states. The integration methods of ODE are mainly divided into three types: explicit method, implicit method and semi implicit method [2].

Because of its simple form, explicit Euler method has been adopted by many researchers in

the vehicle stability control. A coordinated MPC control strategy based on the Euler discretization method for the dynamic wheel torque of 4MIDEV steering is proposed by Peng and Wang et al. [3]. Zhao and Xu et al. propose an energy-efficient MPC Controller for 4WIMD-EVs considering tire slip energy [4]. Clemens and Ricardo propose an algorithm that unifies the wheel slip controller and the torque blending functions into a single framework [5]. Xue and Zheng propose an active collision avoidance system based on MPC [6], in which the Euler method is used for discretization. In spite of its simplicity, integration accuracy of the Euler method is low. Even worse, the integration stability region of the Euler method is quite small. For the short-term prediction time problem such as stability control does not present a problem. However, for problems with long-term prediction time, such as motion control or path following control, it is not ideal. Due to the small step size needed to keep the discretization process stable, a higher computational burden will result.

The most attractive discretization method for linear MPC-based stability control and motion control is the zero-order hold (ZOH) method. Because the ZOH method not only ensures the absolute stability of the discretization process of the system, but also ensures that the state of the discrete system is the same as the state of the continuous system at the discrete time, that is, it is an exact discretization method. The integrated control strategy of path following and lateral motion stabilization for autonomous distributed drive electric vehicles proposed [7] by Zou and Guo et al. is based on the ZOH method. The reconfigurable integrated vehicle stability controller proposed by Amir widely uses the same method [8–11]. Brown and Funke et al. use ZOH method in path tracking strategies based on safe driving envelopes [12]. Ji and Amir propose an MPC-based path planning and tracking algorithm [13], in which the ZOH method is also adopted. Unfortunately, there is no such exact and absolutely stable method for nonlinear systems.

For nonlinear systems, the explicit 4th-order Runge-Kutta (RK4) is a popular method. The RK4 method is used in the NPMC Control based strategy for the stabilization of an electric vehicle proposed by Siampis [14]. Allamaa and Listov et al. present a real-time NPMC strategy with the RK4 method as a discretization method for AVs [15]. The same approach is used in the torque-vectoring controller [16] proposed by Parra and Tavernini. The RK4 method is computationally burdensome and still does not solve the low-speed integration stability problem for the motion control of AVs.

When the vehicle is driven at low speeds, the ordinary differential equations corresponding to nonlinear vehicle dynamics exhibit mild stiffness. This phenomenon causes integration stability problems for motion control or path following control. A common approach to the integration of stiff ODEs is to use an implicit integration method. However, implicit integration methods are usually inefficient and are not a very suitable solution for real-time control. Using the kinematics model can avoid this problem, so many low-speed vehicles use the kinematics model for motion control [17–20]. Because the prediction time of stability control is short, smaller step size can be adopted without affecting the real-time performance. Therefore, the stability control based on NMPC has also been widely studied [14, 16]. Such as, Tavernini and Metzler propose an electric vehicle traction control algorithm based on explicit NMPC [21].

However, the path following problem requires a much longer prediction time, and it is difficult to take too small step size without affecting the real-time performance of the system. Rokonuzzaman and Mohajer propose a controller for AVs based on NMPC [22]. Li and Wang present a nonlinear model predictive path tracking control method considered tire adhesion margin [23]. However, these works are less well described in terms of their implementation details. Guo and Zhang propose a computationally efficient path-following control strategy based on the continuation generalized minimal residual (C/GMRES) algorithm [24]. Owaki and Yuno adopt a similar approach [25]. Parra and Tavernini implemented a 25Hz nonlinear MPC on a real autonomous vehicle [15]. These works show more details, but they do not discuss the integration stability at low speed.

In order to solve the problem of integration stability at low speed, an explicit stabilized RK method is proposed to solve this problem. Explicit stabilized Runge-Kutta (RK) method is an explicit method with extended stability domains along the negative real axis. This method

is proposed by Pieter for the first time [26]. Based on this, a special form of second-order explicit stabilized RK method named Runge-Kutta-Chebyshev (RKC) [27, 28] is proposed. Then a fourth-order method is also proposed [29]. Abdulle summarized these methods and explained them in more detail [30]. The idea of this paper is mainly inspired work of Almuslimani [31], the authors derive stability of RKC with orders one and two for the optimal control of stiff systems. In recent years, other variants of the explicit stabilized RK method have emerged [32, 33].

In addition to solving the Integration stability problem, we use the nonlinear OF-NMPC method to solve the steady-state error problem of motion control based on the linear OF-MPC [34] method we designed previously. For more about OF-MPC theory, these references [35–38] can be referred to. GRAMPC [39, 40] is used as the optimal control solver of the proposed OF-NMPC because it is more efficient and without third-party dependence.

The main highlights of this paper are as follows:

(1) The low-speed integration stability of NMPC based vehicle motion control is revealed. This problem has not been given enough attention for a long time. An efficient stable explicit RK integration method is proposed to solve this problem, which is more efficient than implicit methods.

(2) Based on our previous linear OF-MPC [34], nonlinear OF-MPC is introduced into the motion control of autonomous driving vehicles. The steady-state error is eliminated while the dynamic performance is also improved.

(3) The unscented Kalman filter is used during the introduction of OF-NMPC to fuse the signals from the dynamics model and the positioning device. Finally a smoother state feedback is obtained, effectively suppressing the steering wheel fluctuations.

The rest of this paper is organized as follows. Section 2 describes the OF-NMPC based on GRAMPC, prepares for controller design and integration stability discussions. Section 3 introduces the vehicle motion control modeling and tire model. The specific applications of OF-NMPC in autonomous driving are discussed in Section 4, while low-speed integration stability problems are pointed out, and corresponding solutions are proposed. Section 5 shows the results of the simulation and experiment. Section 6 is conclusions.

2 Nonlinear offset free MPC

2.1 Framework of Nonlinear OF-MPC Control

For the motion control of over-actuated and under-actuated AVs, the linear offset free MPC is discussed in an intensive manner by us [34]. Based on the previous foundation, the use of OF-MPC is extended to nonlinear model predictive control. As shown in Fig.1, the underlying components are similar to linear systems, and typically OF-MPC contains an augmented observer, a reference generator and an MPC or optimal control solver. The difference is that the linear OF-MPC observer uses the Kalman filter while the nonlinear OF-MPC uses the unscented Kalman filter. The linear OF-MPC is based on the OSQP-MPC [34] designed by us, while the solver in this paper is based on the GRAMPC, and we have modified the GRAMPC solver to make it more efficient for motion control problems.

The augmented observer is used to observe states and disturbances. For the autonomous driving motion control problem, the states are fully measurable, but smoother state feedback can be obtained after UKF fusion of vehicle dynamics models. The reference generator is the key to achieving steady-state error-free control. It calculates the reference of control and state based on measurable disturbances, observed obtained unmeasurable disturbances, and state feedback. The nonlinear optimal control is based on the GRAMPC solver, and the GRAMPC source code has been partially modified to improve its real-time performance.

2.2 Nonlinear optimal control problem

In order to solve the optimal control problem in OF-NMPC, the GRAMPC method is used in this paper. It describes the optimal control problem in the following ways,

$$\begin{aligned}\min_{u,p,T} J\left(u,p,T;\ x_0\right) = V(x(T),p,T)+\\ \int_0^T l(x(t),u(t),p,t)\mathrm{d}t\end{aligned} \tag{1}$$

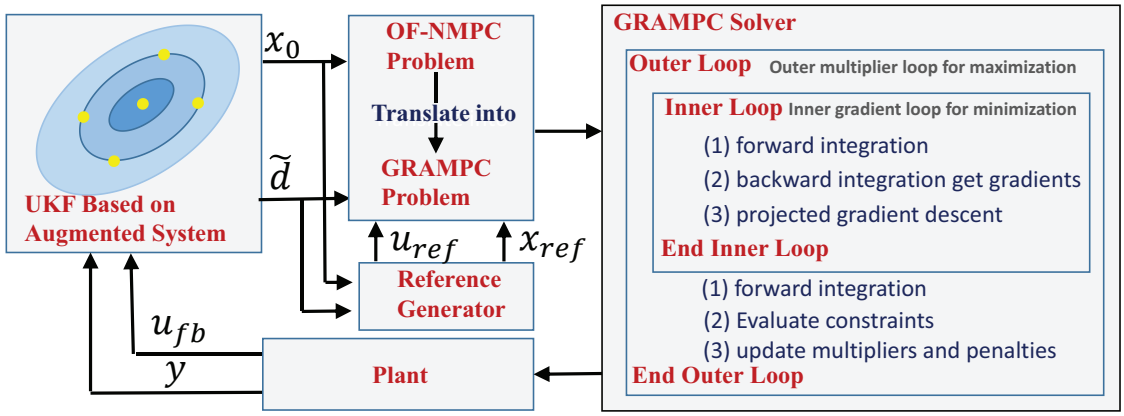

Fig. 1 The overall framework of the OF-NMPC

subject to:

$$\dot{x}(t) = f(x(t), u(t), p, t), x(0) = x_0 \tag{1a}$$
$$g(x(t), u(t), p, t) = 0, g_T(x(T), p, T) = 0 \tag{1b}$$
$$h(x(t), u(t), p, t) \leq 0, h_T(x(T), p, T) \leq 0 \tag{1c}$$
$$u(t) \in [u_{min}, u_{max}] \tag{1d}$$
$$p \in [p_{min}, p_{max}], T \in [T_{min}, T_{max}] \tag{1e}$$

where x is the state, u is the control, p is the parameter, t is time variable, and T is the end time. Equation (1a) are state equation constraints and initial state equation constraints, x_0 is the initial state. Equation (1b) are the equality constraint and terminal equality constraint. Equation (1c) are the inequality constraint and terminal inequality constraint. Equation (1d) is the box constraint for the control variables. Equation (1e) is the box constraint of parameters and end time.

From the description of the problem of GRAMPC, it supports various forms of dynamic system optimization problems. It is possible to use p as optimization variables for the system parameter identification problem. If the terminal time T is used as an optimization variable, it can be used to solve the minimum time problem. If the control variables are used as optimization variables, it is a standard optimal control problem.

The parameter p also plays an important role in the optimal control problem, such as vehicle dynamics parameters, and weight parameters. At the same time, the parameter p and the time variable t together can construct explicit time-varying problems, such as time-varying reference and time-dependent reference models.

The GRAMPC solver can be adapted to various forms of nonlinear optimal control problems, and can also be used to solve OF-NMPC control problems of the following form,

$$\min_u J = \int_0^T l(x(t), u(t), \bar{d}(t), \tilde{d}) \mathrm{d}t \tag{2}$$

subject to:

$$\begin{aligned} &\dot{x}(t) = f\left(x(t), u(t), \bar{d}(t), \widetilde{d}\right) \\ &x(t_0) = x_0 \\ &h\left(x\left(t\right), u\left(t\right), \bar{d}\left(t\right), \widetilde{d}\right) \leq 0 \\ &u(t) \in [u_{min}, u_{max}] \end{aligned}$$

generally, the trajectory of measurable disturbances $\bar{d}$ is known, and unmeasurable disturbances $\widetilde{d}$ need to be observed by filters, so they are assumed to be constant in the prediction time. l is the integral cost. A common integral cost function is shown below,

$$\begin{aligned} l\left(x, u\right) = &\left(x(t) - x_{ref}(t)\right)^{\top} Q\left(x(t) - x_{ref}(t)\right) + \\ &\left(u\left(t\right) - u_{ref}\left(t\right)\right)^{\top} R(u(t) - u_{ref}(t)) \end{aligned} \tag{3}$$

where x_{ref} is the state reference and u_{ref} is the control reference. It can be seen that the state and control reference are also time-varying. The state

and control reference are key factors in realizing no steady-state error control. Similarly to time-varying disturbances, time-varying reference can be described by parameter p and time variable t of GRAMPC.

The GRAMPC is an optimal control solver based on gradient methods. The calculation of the gradient is crucial to it. The adjoint state method is used by it to solve the problem of gradient calculation. The adjoint state method is a numerical method to compute the gradient of a function efficiently. The essential reason for the efficiency of GRAMPC is that the gradient is calculated based on the adjoint sensitivity analysis method. The gradient is calculated by the backward integration of the adjoint states. Hence GRAMPC comprises the integration of two state equations, one for the simulation of the original state equation and the other for calculating the gradient.

The integration stability of the adjoint state equation is the same as the original system, and to argue this in the subsequent sections we need to introduce the Hamiltonian function,

$$H(\boldsymbol{x},\boldsymbol{u},\boldsymbol{p},\boldsymbol{\lambda},t,\boldsymbol{\mu},\boldsymbol{c}) = \bar{l}(\boldsymbol{x},\boldsymbol{u},\boldsymbol{p},t,\boldsymbol{\mu},\boldsymbol{c}) + \boldsymbol{\lambda}^{\top}\boldsymbol{f}(\boldsymbol{x},\boldsymbol{u},\boldsymbol{p},t) \tag{4}$$

where $\bar{l}$ is augmented integration cost term, which can refer to [39, 40]. Then the definition of the adjoint state is as follows,

$$\begin{aligned}\dot{\lambda} &= -H_x(\boldsymbol{x},\boldsymbol{u},\boldsymbol{p},\lambda,t,\boldsymbol{\mu},\boldsymbol{c})\\ \lambda(T) &= \bar{V}_x\left(\boldsymbol{x}(T),\boldsymbol{p},T,\boldsymbol{\mu}_T,\boldsymbol{c}_T\right)\end{aligned} \tag{5}$$

It is not difficult to see that the equation of the adjoint state is a linear equation, where $\boldsymbol{x}$ is calculated from the forward integration of the original equation of state.

2.3 Reference generator and Kalman filter

The reference generator of OF-NMPC should satisfy the nonlinear equations described by Equation (6) as much as possible. It is easy to see that it is actually the steady-state of the equation of state, i.e., the derivative of the state is zero.

$$f\left(x_{ref}(t),u_{ref}(t),\bar{d}(t),\widetilde{d}\right) = 0 \tag{6}$$

However, the above nonlinear equations may not have real roots, in order to solve this problem, the equations can be relaxed. However, the relaxation scheme for nonlinear systems is usually determined by the specific problem, so this issue will be left to be discussed in following section.

The filter used in this paper is UKF, and the original state equation will not be used directly, but based on its augmented form,

$$\begin{bmatrix}\dot{x}\\ \dot{\widetilde{d}}\end{bmatrix} = \begin{bmatrix}f\left(x_e,u_e\right)\\ 0\end{bmatrix} \tag{7}$$

where $x_e = [x,\widetilde{d}]$ is the augmented state and variable $u_e = [u,\bar{d}]$ is the augmented control variable. It can be seen that Equation (7) is based on the disturbance invariance assumption. Since OF-NMPC is introduced to eliminate steady-state errors, this assumption is reasonable. In fact, as long as the filter converges fast enough, it is able to observe disturbances that change slowly. Further verification will appear in the simulation section.

3 Modeling of AVs

3.1 Modeling of tires

For the lateral motion of the tire, the dugoff [41] tire model is adopted,

$$F_y = \begin{cases} -C_\alpha \tan\alpha, |\tan\alpha| < \mu F_z^N/\left(2C_\alpha\right)\\ sign\left(\alpha\right)\mu F_z^N[1-\mu F_z^N(4C_\alpha\left|tan\alpha\right|)], otherwise\end{cases} \tag{8}$$

where α is the tire side angle, C_α is the tire lateral stiffness, μ and F_z^N are the rated friction and load, respectively. However, the stiffness of the dugoff model does not consider the influence of tire load. Based on the results of the TMeasy tire model [42], we introduce the influence of load on tire stiffness.

$$\begin{aligned}C_\alpha\left(F_z\right) = \tfrac{F_z}{F_z^{\mathrm{N}}}\{2C_\alpha\left(F_z^{\mathrm{N}}\right) - \tfrac{1}{2}C_\alpha\left(2F_z^{\mathrm{N}}\right) -\\ \left[C_\alpha\left(F_z^{\mathrm{N}}\right) - \tfrac{1}{2}C_\alpha\left(2F_z^{\mathrm{N}}\right)\right]\tfrac{F_z}{F_z^{\mathrm{N}}}\}\end{aligned} \tag{9}$$

The lateral dugoff tire model is reversible, i.e., the lateral side slip angle can be calculated in reverse based on the lateral force, which is important for the reference generation of the OF-NMPC. The reversible tire model allows obtaining the reference in the form of an analytical solution, while avoiding to solve the nonlinear equations.

3.2 Modeling of vehicle dynamics

First, the naming rule for variables is declared to facilitate modeling and avoid redundant definitions. The superscript $\bar{}$ represents the value or measurable disturbances of relevant variables at the current time. Such as $\bar{\delta}_f$ represents the front wheel angle at the current time. The superscript $\tilde{}$ represents the unmeasurable disturbances of relevant variables. The superscript $\hat{}$ represents the references of relevant variables.

The tire parameters and vehicle parameters used in the modeling are shown in Table1. These parameters are consistent in the simulation and real vehicle experiments in the subsequent sections.

Table 1 Nominal vehicle parameters

Symbol	Definition	Value
m	Vehicle mass	2050 kg
$C_{\alpha f}\left(F_z^N\right)$	Lateral stiffness of front axle under rating tire load	61000 N/rad ×2
$C_{\alpha r}\left(F_z^N\right)$	Lateral stiffness of rear axle under rating tire load	61000 N/rad ×2
$C_{\alpha f}\left(2F_z^N\right)$	Lateral stiffness of front axle under two times rating tire load	120000 N/rad ×2
$C_{\alpha r}\left(2F_z^N\right)$	Lateral stiffness of rear axle under two times rating tire load	120000 N/rad ×2
F_{zf}^N	Front axle rating tire load	3187 N ×2
F_{zr}^N	Rear axle rating tire load	3187 N ×2
x_f	Distance from front axle to c.g.	1. 375 m
x_r	Distance from rear axle to c.g	-1. 375 m
ρ_{bf}	braking distribution ratio of front axle	0.625
ρ_{br}	braking distribution ratio of rear axle	0.375
δ_{fmax}	Maximum steering angle of front wheel	40°
I_z	Z-axis moment of inertia	1800 kg·m²

As shown in Fig.2, it is a single-track model of a front-wheel drive vehicle front-wheel steering vehicle.

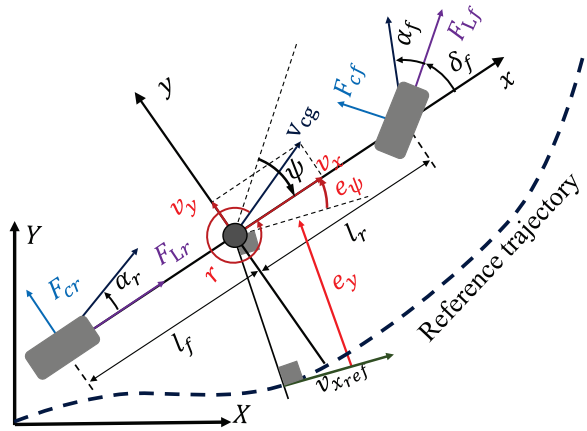

Fig. 2 Single-Track vehicle model and road model

The vehicle three degree of freedom model is adopted here, and its dynamic equation is as follows,

$$\begin{cases} \dot{v}_x = v_y r + \left(F_{xf}\cos\delta_f + F_{xr} - F_{yf}\sin\delta_f\right)/m + \tilde{a}_{xd} \\ \dot{v}_y = -v_x r + \left(F_{yf}\cos\delta_f + F_{xf}\sin\delta_f + F_{yr}\right)/m + \tilde{a}_{yd} \\ \dot{r} = \left(x_f F_{yf} + x_r F_{yr}\right)/I_z + \tilde{r}_d \end{cases} \tag{10}$$

where m is the mass of the whole vehicle, I_z is the moment of inertia of the yaw, v_x and v_y are the longitudinal and lateral speed, r is the yaw rate, F_{xf} and F_{xr} are the longitudinal force of the front wheel and the rear wheel respectively, F_{yf} and F_{yr} are the lateral force of the front wheel and the rear wheel respectively, δ_f is the angle of the front wheel, $\widetilde{a}_{xd}$ and $\widetilde{a}_{yd}$ are the unmeasurable longitudinal and lateral disturbing acceleration, and $\widetilde{r}_d$ is yaw disturbing angular acceleration, x_f and x_r are the x coordinates of the front and rear axles at the vehicle coordinate system, respectively.

The lateral forces are calculated by the dugoff tire model,

$$F_{yi} = F_{yi}(\tan\alpha_i), i \in f, r \tag{11}$$

and,

$$\begin{aligned} \tan\alpha_i = \tan(\beta_i - \delta_i) &= \left[\left(v_y + x_i\dot{r}\right)/\left(v_x - y_i\dot{r}\right)\right] - \delta_i \\ &\approx \left(v_y + x_i r\right)/v_x - \delta_i, i \in f, r \end{aligned} \tag{12}$$

Under the assumption of small steering angle, it can be simplified to the following form,

$$\begin{cases} \dot{v}_x = a_x + a_{xd} \\ \dot{v}_y = -v_x r + \left(F_{yf} + F_{yr}\right)/m + a_{yd} \\ \dot{r} = \left(x_f F_{yf} + x_r F_{yr}\right)/I_z + r_d \end{cases} \tag{13}$$

where,

$$a_x = a_{xf} + a_{xr}, a_{xf} = F_{xf}/m, a_{xr} = F_{xr}/m \tag{14}$$

For longitudinal disturbance,

$$\begin{cases} \bar{a}_{xd} = \left[\bar{F}_{Lf}\left(\cos\bar{\delta}_f - 1\right) - \bar{F}_{Cf}\sin\bar{\delta}_f\right]/m + \bar{v}_y\bar{r} \\ a_{xd} = \tilde{a}_{xd} + \bar{a}_{xd} \end{cases} \tag{15}$$

For lateral disturbance,

$$\begin{cases} \bar{a}_{yd} = \left[\bar{F}_{yf}\left(\cos\bar{\delta}_f - 1\right) - \bar{F}_{xf}\sin\bar{\delta}_f\right]/m \\ a_{yd} = \tilde{a}_{yd} + \bar{a}_{yd} \end{cases} \tag{16}$$

For yaw motion disturbance,

$$\begin{cases} \bar{r}_d = x_f \bar{F}_{yf} \left(\cos \bar{\delta}_f - 1\right) / I_z \\ r_d = \bar{r}_d + \tilde{r}_d \end{cases} \tag{17}$$

The change of tire vertical load is related to longitudinal acceleration and meets the following relationship,

$$F_{z_f} = m(-x_r g - ah)/(x_f - x_r) \tag{18}$$

$$F_{z_r} = m(x_f g + ah)/(x_f - x_r) \tag{19}$$

As shown in Fig.2, e_y is the distance from the center of gravity of the vehicle to the centerline of the lane, and e_ψ is the orientation error of the vehicle for the road, then,

$$e_\psi = \psi - \psi_{ref} \tag{20}$$

$$\dot{e}_\psi = r - \kappa v_x \tag{21}$$

$$e_{\psi_d} = \bar{e}_{\psi_d} + \widetilde{e}_{\psi_d} = \widetilde{e}_{\psi_d} \tag{22}$$

ψ and ψ_{ref} are heading angle and reference heading angle respectively, κ is the curvature of reference trajectory, and e_{ψ_d} is the yaw angle error disturbance.

$$\dot{e}_y = v_y cose_\psi + v_x sine_\psi + \widetilde{e}_{y_d} = v_y + v_x e_\psi + e_{y_d} \tag{23}$$

$$\begin{cases} \bar{e}_{y_d} = \bar{v}_y \left(\cos \bar{e}_\psi - 1\right) + \bar{v}_x \left(\sin \bar{e}_\psi - \bar{e}_\psi\right) \\ e_{y_d} = \bar{e}_{y_d} + \tilde{e}_{y_d} \end{cases} \tag{24}$$

and e_{y_d} is the lateral error disturbance.

In order to facilitate the analysis of integration stability and the calculation of gradient for GRAMPC, it is necessary to give the Jacobian matrix of the state equation to the state and control. The Jacobian matrix of the state is,

$$A = \begin{bmatrix} 0 & 0 & 0 & 0 & 0 \\ \frac{\sum \widetilde{C}_{\alpha i} \frac{\partial \alpha_i}{\partial v_x}}{m} - r & \frac{\sum \widetilde{C}_{\alpha i} \frac{\partial \alpha_i}{\partial v_y}}{m} & \frac{\sum \widetilde{C}_{\alpha i} \frac{\partial \alpha_i}{\partial r}}{m} - v_x & 0 & 0 \\ \frac{\sum x_i \widetilde{C}_{\alpha i} \frac{\partial \alpha_i}{\partial v_x}}{I_z} & \frac{\sum x_i \widetilde{C}_{\alpha i} \frac{\partial \alpha_i}{\partial v_y}}{I_z} & \frac{\sum x_i \widetilde{C}_{\alpha i} \frac{\partial \alpha_i}{\partial r}}{I_z} & 0 & 0 \\ e_\psi & 1 & 0 & 0 & v_x \\ -\kappa & 0 & 1 & 0 & 0 \end{bmatrix} \tag{25}$$

The Jacobian matrix of the control is,

$$B = \begin{bmatrix} 0 & \frac{\widetilde{C}_{\alpha f}}{m} \frac{\partial \alpha_f}{\partial \delta_f} & \frac{x_f \widetilde{C}_{\alpha f}}{I_z} \frac{\partial \alpha_f}{\partial \delta_f} & 0 & 0 \\ 1 & 0 & 0 & 0 & 0 \end{bmatrix}^T \tag{26}$$

where,

$$\partial \alpha_i / \partial v_x = \alpha_i / v_x, \partial \alpha_i / \partial v_y = 1/v_x, \partial \alpha_i / \partial r = x_i / v_x \tag{27}$$

$$\widetilde{C}_{\alpha i} = \frac{\partial F_{yi}}{\partial \tan \alpha_i} = \begin{cases} -C_\alpha, |tan\alpha| < \mu \bar{F}_z^N / (2C_\alpha) \\ sign(\alpha) \left(\mu F_z^N\right)^2 / 4 C_\alpha (tan\alpha)^2, \text{ otherwise} \end{cases} \tag{28}$$

3.3 Constraints of dynamics model

For longitudinal control, the maximum capacity of the motor and brake actuator is limited, so the maximum acceleration and braking deceleration are limited, meeting the following relationship,

$$a_{xmin} \le a_x \le a_{xmax} \tag{29}$$

The maximum steering angle and maximum steering rate of the steering system are also limited,

$$|\delta_f| \le \delta_{fmax} \tag{30}$$

$$|\omega_f| \le \omega_{fmax} \tag{31}$$

Maintaining the stability of the vehicle in the motion control of autonomous driving vehicles is also an important research content of motion control. Generally, these stability conditions are related to tires. For example, many research work uses the maximum sideslip angle of tires as the stability condition. However, the maximum sideslip angle is related to the longitudinal force of the tire. In this paper, a concept similar to the tire friction circle is used to establish the stability conditions. The following relationship shall be met for both tires on the front and rear axles,

$$\left(\alpha_i / \alpha_{imax}\right)^2 + \left(a_{xi} / a_{ximax}\right)^2 \le 1, i \in f, r \tag{32}$$

However, using the above constraints directly will lead to a problem. The problem is that front and rear wheel brakes are not independent, if the above constraints are directly used, the problem will become a mixed-integer optimization problem. In order to avoid this problem, a further derivation is necessary. Next, the constraint will be directly mapped to the front, rear wheel side slip angle and the total longitudinal acceleration. Thanks to the first-order method used by GRAMPC, we only need to ensure that the constraints are first-order continuous. Assume that

ρ_f and ρ_r are the ratio of front and rear axles of total acceleration respectively, and, ρ_{bf} and ρ_{br} are the braking acceleration distribution ratio respectively, then,

$$\rho_f = \begin{cases} 1, & a_x \geq 0 \\ \rho_{bf}, & a_x < 0 \end{cases}, \rho_r = \begin{cases} 0, & a_x \geq 0 \\ \rho_{br}, & a_x < 0 \end{cases} \tag{33}$$

Then Equation (32) can be transformed into the following constraints,

$$\left(\alpha_i/\alpha_{imax}\right)^2 + \left(\rho_i a_x/a_{ximax}\right)^2 \leq 1, i \in f, r \tag{34}$$

This constraint is shown in Fig.3 and the continuity of its first derivative can be guaranteed.

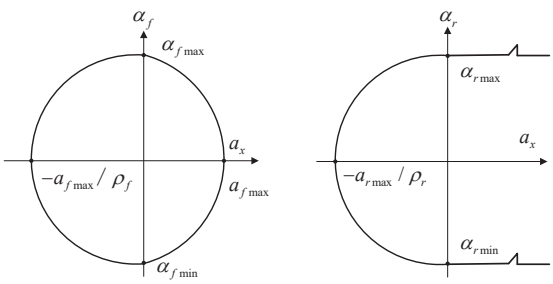

(a) Front tire friction map to state and control space

(b) Rear tire friction map to state and control space

Fig. 3 Tire friction circle mapped to control and state

The gradient information of constraint is also necessary for GRAMPC. The Jacobian matrix of constraint to state is,

$$h_x = \begin{bmatrix} \frac{2\alpha_f}{\alpha_{fmax}^2}\frac{\partial\alpha_f}{\partial v_x} & \frac{2\alpha_f}{\alpha_{fmax}^2}\frac{\partial\alpha_f}{\partial v_y} & \frac{2\alpha_f}{\alpha_{imax}^2}\frac{\partial\alpha_f}{\partial r} & 0 & 0 \\ \frac{2\alpha_r}{\alpha_{rmax}^2}\frac{\partial\alpha_r}{\partial v_x} & \frac{2\alpha_r}{\alpha_{rmax}^2}\frac{\partial\alpha_r}{\partial v_y} & \frac{2\alpha_r}{\alpha_{rmax}^2}\frac{\partial\alpha_r}{\partial r} & 0 & 0 \end{bmatrix} \tag{35}$$

The Jacobian matrix of constraint to control is,

$$h_u = \begin{bmatrix} \frac{2\alpha_f}{\alpha_{fmax}^2}\frac{\partial\alpha_f}{\partial\delta_f} & 2\rho_f^2 a_x/a_{fmax}^2 \\ 0 & 2\rho_r^2 a_x/a_{rmax}^2 \end{bmatrix} \tag{36}$$

where $\partial\alpha_f/\partial\delta_f = -1$.

4 OF-NMPC design

4.1 Reference state and control

As stated in Section 2, the derivative of the state in the steady state should be zero,

$$\hat{a}_x = -a_{xd} \tag{37}$$

$$\hat{F}_{y_{fre}} + \hat{F}_{y_r} = m a_{y_{ref}} \tag{38}$$

$$x_f \hat{F}_{y_f} + x_r \hat{F}_{y_r} + I_z r_d = 0 \tag{39}$$

where,

$$a_{y_{ref}} = v_x r_{ref} - a_{y_d} \tag{40}$$

and r_{ref} is reference yaw rate of reference path. Then,

$$\hat{F}_{y_f} = \frac{-x_r m a_{y_{ref}}}{x_f - x_r} - \frac{I_z r_d}{x_f - x_r} \tag{41}$$

$$\hat{F}_{y_r} = \frac{x_f m a_{y_{ref}}}{x_f - x_r} + \frac{I_z r_d}{x_f - x_r} \tag{42}$$

However, using the above method to obtain the reference value may violate the stability constraint. To avoid this problem, relaxation factors $\lambda \in (0, 1]$ for lateral and longitudinal acceleration requirements are introduced,

$$\hat{a}_x = -\lambda a_{xd} \tag{43}$$

$$\hat{F}_{y_f} + \hat{F}_{y_r} = \lambda m a_{y_{ref}} \tag{44}$$

$$x_f \hat{F}_{y_f} + x_r \hat{F}_{y_r} + I_z r_d = 0 \tag{45}$$

The relaxation factor λ should be as large as possible when equality constraints and inequality constraints are satisfied. If only lateral constraints are considered,

$$\left|\hat{F}_{y_f}\right| \leq F_{yf_{max}} \tag{46}$$

$$\left|\hat{F}_{y_r}\right| \leq F_{yr_{max}} \tag{47}$$

Then we get the following relationship,

$$F_t = m(v_x r_{ref} - a_{y_d}) \tag{48}$$

$$\lambda'_{max} = \begin{cases} \min\left[\frac{\mu F_{z_f}\left(x_f - x_r\right) + I_z r_d}{max\left\{-x_r m a_{y_{ref}}, \epsilon\right\}}, \frac{\mu F_{z_r}\left(x_f - x_r\right) - I_z r_d}{max\left\{x_f m a_{y_{ref}}, \epsilon\right\}}\right], F_t \geq 0 \\ \min\left[\frac{-\mu F_{z_f}\left(x_f - x_r\right) + I_z r_d}{\min\left\{-x_r m a_{y_{ref}}, -\epsilon\right\}}, \frac{-\mu F_{z_r}\left(x_f - x_r\right) - I_z r_d}{\min\left\{x_f m a_{y_{ref}}, -\epsilon\right\}}\right], F_t < 0 \end{cases} \tag{49}$$

$$\lambda_{max} = \max[\min\left(\lambda'_{max}, 1\right), 0] \tag{50}$$

After calculating the reference tire lateral force, the sideslip angle can be obtained using the

tire lateral inverse model. And the sideslip angle of the front and rear wheels satisfies the following relationship,

$$\begin{cases} tan(\hat{\alpha}_f) = (\hat{v}_y + x_f\hat{r})/v_x - \hat{\delta}_f \\ tan(\hat{\alpha}_r) = (\hat{v}_y + x_r\hat{r})/v_x \end{cases} \tag{51}$$

where $\hat{r} = \lambda_{max} r_{ref}$, then,

$$\hat{v}_y = v_x tan(\hat{\alpha}_r) - x_r\hat{r} \tag{52}$$

$$\hat{\delta}_f = [v_x tan(\hat{\alpha}_r) - x_r\hat{r} + x_f\hat{r}]/v_x - tan(\hat{\alpha}_f) \tag{53}$$

It can be seen from Equation (52) that in the steady-state, the lateral velocity $\hat{v}_y$ is not equal to zero, and the velocity at the mass center should be tangent to the reference trajectory, which means that the heading angle error is not zero in the steady-state, and the following relationship is satisfied,

$$\tan \hat{e}_\psi = -\hat{v}_y/v_x \tag{54}$$

The lateral error reference should be zero,

$$\hat{e}_\psi = 0 \tag{55}$$

The longitudinal speed reference is time-varying and satisfies the following relationship,

$$\hat{v}_x = \hat{v}_{x0} + \hat{a}_x t \tag{56}$$

where $\hat{v}_{x0}$ is the reference speed at the current time, t is the predicted time.

4.2 Stability problem of the explicit RK method

Neither the direct nor the indirect optimal control methods rely on integrators to discretize the dynamic system. Thus, the stability of the integrator is crucial, and an unstable integrator cannot only accurately predict the future trajectory of the system, but even affects the stability of the closed-loop system. Using integration stability theory, the low-speed integration stability problem in vehicle lateral motion control will be revealed by us.

The analysis of integration stability for the one-step method is usually based on the following Dahlquist test equation,

$$\dot{y} = \lambda y, y(0) = y_0 \tag{57}$$

Any kind of single-step integrator can be substituted into the above equation to obtain the following discrete relationship,

$$y_{k+1} = R(h\lambda)y_k \tag{58}$$

let $z = h\lambda$, then $R(h\lambda)$ is the stability function of the corresponding integrator. The Dahlquist test equations are meaningful for general nonlinear systems. Because any nonlinear system at a given state can get its linearized form, the linearized Jacobian matrix can be transformed into Jordan or diagonal form. This means that λ of the Dahlquist test equation represents the eigenvalues of the Jacobian matrix. Therefore, in order to avoid y_k divergence, the following relationship needs to be satisfied,

$$|R(z)| \leq 1 \tag{59}$$

According to Equation (10), it can be seen that Jacobian matrices of the adjoint state system and the original system are the same, so we only need to discuss the stability of the original system. The stability function of the explicit Runge Kutta method of order p is as follows,

$$R(z) = 1 + z + z^2/2! + \ldots + z^p/p! \tag{60}$$

Generally, when the integrator is stable, we want to use a larger step size to realize the integration process of NMPC, because it can obtain higher computational efficiency. The quantitative calculation method of the maximum step size meeting the stability requirements will be given in this section.

The Jacobian matrix of the state equation for lateral motion control is described in Equation (25). There are two non-zero eigenvalues, which can be derived using the following equation,

$$\lambda_1 = (A_{11} + A_{22}) - [(A_{11} - A_{22})^2 + 4A_{12}A_{21}]^{1/2} \tag{61}$$

$$\lambda_2 = (A_{11} + A_{22}) + [(A_{11} - A_{22})^2 + 4A_{12}A_{21}]^{1/2} \tag{62}$$

It can be seen that the eigenvalues are only related to the vehicle speed and tire stiffness. The qualitative conclusion is that the greater the stiffness of the tire and the lower the speed of the vehicle, the greater the stiffness of the ODE equation.

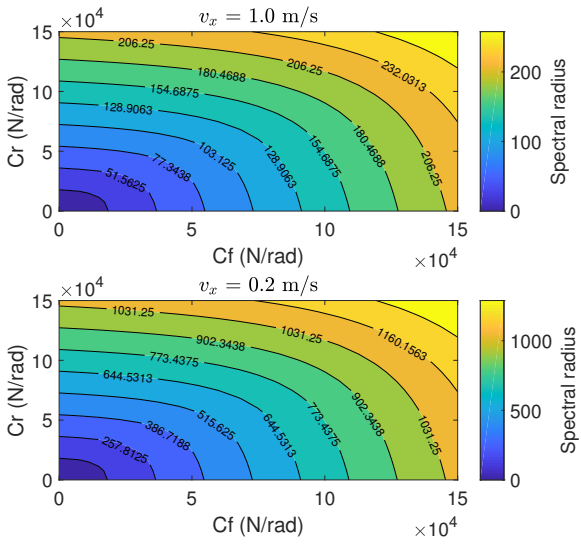

Fig. 4 Spectral radius of vehicle dynamics equation

As shown in Fig.4, the above and below subplots are the spectral radius of the prediction model at vehicle speeds of 1.0m/s and 0.2m/s, respectively. The spectral radius reaches more than 250 at 1m/s and up to 1200 at 0.2m/s. If the explicit RK method is used directly, a small integration step is required to ensure the stability of the integration. This phenomenon is the low-speed integration stability problem of NMPC for AVs.

4.3 RKC method for NMPC of AVs

The same low-speed integration stability problems of AVs motion control exist when using linear MPCs. However, the problem is better handled in linear systems. For linear systems, implicit methods usually exist analytic solutions, and methods for exact solutions still exist, such as the zero-order hold method. However, the computational burden associated with using implicit methods in nonlinear systems is considerable.

It is observed that the eigenvalue trajectories of the lateral vehicle dynamics model are concentrated around the negative real axis. Therefore, using the RKC method would be a good choice. The RKC methods are explicit one-step methods with an extended stability domain that grows quadratically with the number of stages s of the method along the negative real axis. The stable region expands with the square of the stages along the negative real axis. More specifically, the first-order RKC method is used because it is less computationally burdensome compared to higher-order methods while maintaining the same stability region. And it is more frequently used in scenarios where the integration accuracy is not very high, but the real-time performance is more critical.

$$dy/dt = F(y,t) \tag{63}$$

For a nonlinear ordinary differential equation as described in Equation (63), the RKC method for the first-order s-stage is defined as follows,

$$y_{k0} = y_k, y_{k1} = y_k + \mu_1 h F(y_{k0}, 0) \tag{64}$$

$$\begin{aligned} y_{ki} = \mu_i h F(y_{k,i-1}, t_{k,i-1}) + \nu_i y_{k,i-1} + \\ (1-\nu_i) y_{k,i-2}, i = 2, \ldots, s \end{aligned} \tag{65}$$

$$y_{k+1} = y_{ks} \tag{66}$$

where h is the integration step size,

$$\mu_i = \frac{2\omega_1 T_{i-1}(\omega_0)}{T_i(\omega_0)}, \nu_i = \frac{2\omega_0 T_{i-1}(\omega_0)}{T_i(\omega_0)} \tag{67}$$

and,

$$\omega_0 = 1 + \frac{\eta}{s^2}, \omega_1 = \frac{T_s(\omega_0)}{T_s'(\omega_0)}, \mu_1 = \frac{\omega_1}{\omega_0} \tag{68}$$

$$t_{k,0} = \mu_1, t_{k,1} = \mu_1 \tag{69}$$

$$t_{k,i-1} = \mu_{i-1} + \nu_{i-1} t_{k,i-2} + (1-\nu_{i-1}) t_{k,i-3} \tag{70}$$

where η is called the damping parameter, T is the Chebyshev polynomials and satisfies the following recurrence relation,

$$T_j(z) = 2zT_{j-1}(z) - T_{j-2}(z) \tag{71}$$

and $T_1(z) = 1.0$, $T_2(z) = z$.

All these parameters mentioned above can be calculated offline, so although the first-order RKC method looks complicated, in fact, its computational burden is small.

The integration stability function of the first-order RKC method is as follows,

$$R_s(z) = T_s\left(1 + z/s^2\right) \tag{72}$$

As shown in Fig.5, the stability regions of the RKC method with stages of 5, 6, 7, Euler method and RK5 are demonstrated. The $x-y$ plane as shown represents the complex plane of variable

z. The colored straight line represents the trajectory of the z-variable at different speeds when the integration step size is 0.05s, and the color bar represents the speed.

It can be seen that the stability region of the RKC method is greatly extended. The stability region of RKC-5 is expanded by more than a factor of 15 compared with RK5, while with comparable computational burden. Meanwhile RK methods are far from meeting the integration stability requirements at low speed.

5 Results and discussions

5.1 Simulation of 6m radius U-turn maneuver

One of the topics of this paper is to address the issue of integration stability at low speeds. In order to verify the validity of the proposed RKC integrator, the 6th order RK method and the RKC method are compared under the maneuver with a radius of 6 m and a vehicle speed of 0.2 m/s. The 6th order RK method and the RKC method have the same computational burden.

It can be seen from Fig.6 that the controller of the 6th order RK method undergoes obvious oscillation and instability, and the lateral error is not controlled. The opposite is true for the 6th order RKC method, where the maximum lateral error is about 20 cm. This is the same as the results obtained in our previous section, the RKC method is able to obtain a larger stability region with the same computational burden as the RK method.

5.2 Simulation of 50m radius U-turn maneuver

The UKF is introduced for two purposes, one is to fuse the positioning signals of AVs to obtain positioning results with higher confidence and less noise, and the other is to observe the prediction model disturbances caused by model mismatch and external disturbances, thus eliminating steady-state errors.

As described in Equation (7), the dimension of the augmented state equation for UKF is 10, and the dimension of the measurement equation is 5. Obviously, it is not a very simple issue to determine the variance of the state equation and the measurement. To facilitate the observation of the convergence rate and noise of the disturbances, a 50m radius U-turn maneuver is designed. The U-turn maneuver has two curvature step points, and the vehicle is in steady-state before and after the step point, so it is ideal for observing the convergence rate of the filter. The straight-line and uniform circular motion parts are also very useful for observing whether the steady-state error is eliminated.

Usually, the localization signal in an actual AVs gives the variance of the measurement directly. What needs to be determined is the variance of the vehicle dynamics equation, which is a 5-dimensional vector. The smaller the variance of this part, the smaller the variance or noise of the fused state, but too small can easily lead to bias and lag of the signal. The last part is the variance of the disturbances of the augmented state equation. The larger the variance of the disturbances, the faster the convergence rate and the more immediate the compensation of the disturbances, but too large may lead to too much noise of the disturbances and affect the control performance.

After parameter tuning based on the basic criterion described above, the standard deviation of the augmented equation of state is,

$$\sigma_{x_e} = diag([1, 1, 1, 1, 1, 200, 200, 200, 1, 1]) \times 10^{-4}$$

The standard deviation of the measurement is,

$$\sigma_y = [0.01, 0.01, 0.005, 0.01, 0.005]$$

And the MPC weighting parameters as described in Table2 are obtained.

Table 2 MPC parameters

Symbol	Definition	Quantity
$Nhor$	Number of discretization points	21
$Thor$	Prediction horizon	1s
W_{vx}	Weight of vehicle longitudinal speed	1.0
W_{v_y}	Weight of vehicle lateral speed	0.0
W_r	Weight of yaw rate	1.0
W_{e_y}	Weight of lateral error	1.0
W_{e_ψ}	Weight of heading error	0.5
W_{δ_f}	Weight of front wheel steering angle	10.0
W_a	Weight of longitudinal acceleration	1.0
α_{fmax}	Maximum side slip angle of front wheel	12°
α_{rmax}	Maximum side slip angle of rear wheel	12°
δ_{fmax}	Maximum steering angle	40°

To illustrate the role of the filter, two controllers were designed. They are OF-NMPC and

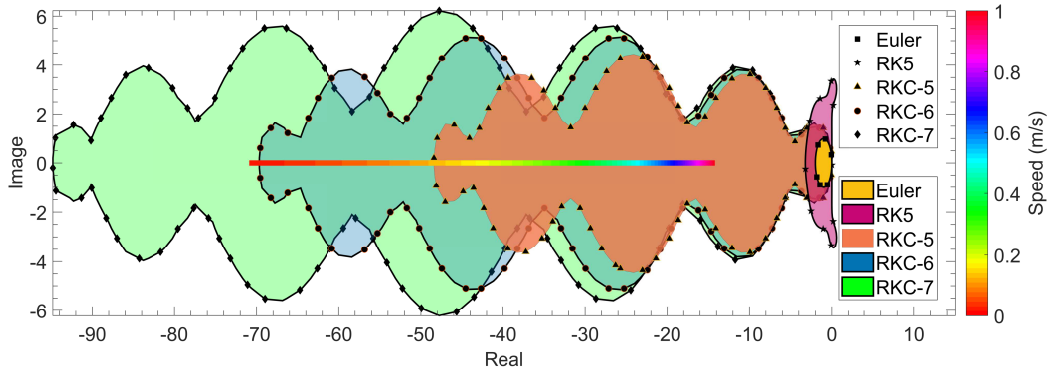

Fig. 5 Stability region of RK and RKC methods

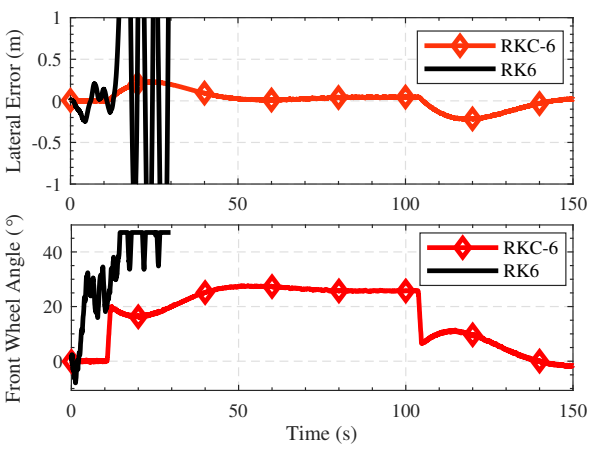

Fig. 6 Simulation results of 6m radius U-turn maneuver

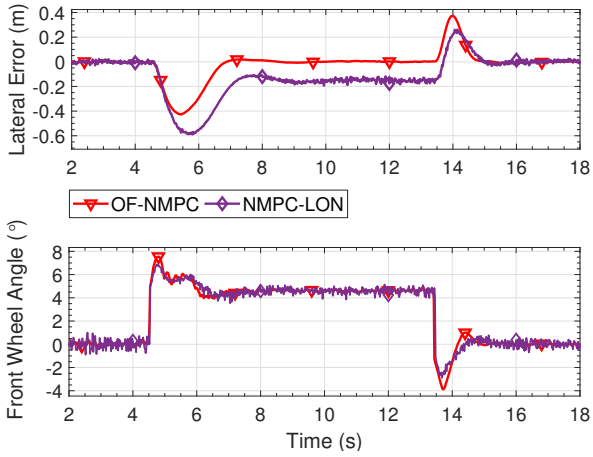

Fig. 7 Simulation results of 50m radius U-turn maneuver under the speed of 18m/s

NMPC-LON. The OF-NMPC compensates lateral and longitudinal disturbances using state feedback fusing dynamic equations. In contrast, the NPMC-LON compensates only the longitudinal disturbance, and does not use the fused feedback. NMPC-LON uses longitudinal compensation in order to be comparable with OF-NMPC in lateral control, otherwise, it is meaningless to compare lateral errors when vehicle speeds are different.

As shown in Fig.7, the lateral error signal of OF-MPC becomes smoother after the UKF filter fuses the vehicle dynamics model, while the lateral error noise of NMPC-LON is relatively large. It can also be seen that the lateral steady-state of OF-NMPC is eliminated when the vehicle enters the circular motion, while the steady state lateral error of NMPC-LON is about 18 cm. Meanwhile, in the non-steady-state, the maximum lateral error of NMPC-LON reaches about 60cm,

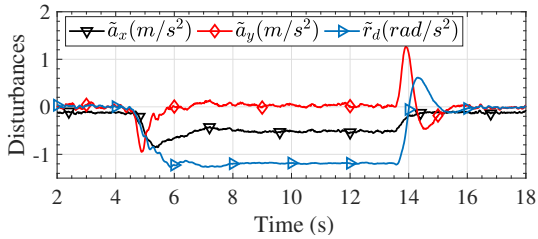

Fig. 8 Disturbance observation of 50m radius U-turn maneuver under the speed of 18m/s

while that of OF-NMPC is about 40cm. Meanwhile, because the feedback noise of NMPC-LON is not smoothed, its front-wheel steering control fluctuations are more dramatic, while the opposite is true for OF-NMPC.

The results of the UKF disturbance observations are shown in Fig.8, which shows that the convergence rate of the filter is appropriate,

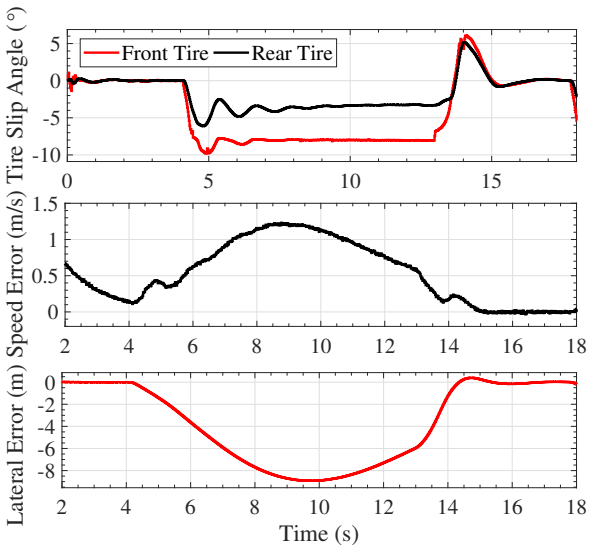

Fig. 9 Simulation results of 50m radius U-turn maneuver under the speed of 21m/s

and the fluctuations of the disturbance observations are controlled within a certain range. Due to the presence of steering, longitudinal acceleration disturbances increase as the vehicle enters the circular motion state and reaches 0.5 m/s^2. As the front wheel needs to provide longitudinal force, it makes the lateral stiffness of the front wheels change, which causes the mismatch of the yaw motion, and the yaw angular acceleration disturbance reaches 1.2 rad/s^2.

Further increase the target speed to 21m/s, if the longitudinal speed is accurately controlled, the lateral acceleration will reach 8.82m/s, while the adhesion coefficient of the road surface in the simulation is 0.85, which is obviously beyond the adhesion limit. And the longitudinal force also exists in order to maintain the speed, which will make the situation further deteriorated. From Fig.9, it can be seen that the front wheel lateral side slip angle is at the maximum value for a long time, which demonstrates the effectiveness of the tire side slip angle constraint. In order to avoid losing stability, a significant active deceleration occurs. Despite the large lateral and longitudinal speed errors, the vehicle can still remain stable and avoid further deterioration of the situation. Eventually the lateral error is controlled again after the vehicle was driven out of the curve and back into the straight section.

5.3 Simulation of DLC maneuver

The purpose of the introduction of OF-NMPC is to eliminate the steady-state error, nevertheless its effect on the dynamic performance is still uncertain. In order to verify the dynamic performance of OF-NMPC, the double lane change (DLC) maneuver is designed. The trajectory of DLC maneuver is as follows,

$$\psi_{ref}(X) = \frac{d_{y_1}}{2}(1+tanh(z_1)) - \frac{d_{y_2}}{2}(1+tanh(z_2)) \tag{73}$$

$$Y_{ref}(X) = arctan\left(d_{y_1}\left(\frac{1}{cosh(z_1)}\right)^2\left(\frac{1.2}{d_{x_1}}\right) - d_{y_2}\left(\frac{1}{cosh(z_2)}\right)^2\left(\frac{1.2}{d_{x_2}}\right)\right) \tag{74}$$

In the simulation, the parameters are shown as follows,

$z_1 = (2.4/25)(X-27.19)-1.2, d_{x1} = 25, d_{y1} = 5.0,$

$z_2 = (2.4/25)(X-54.38)-1.2, d_{x2} = 25, d_{y2} = 5.0.$

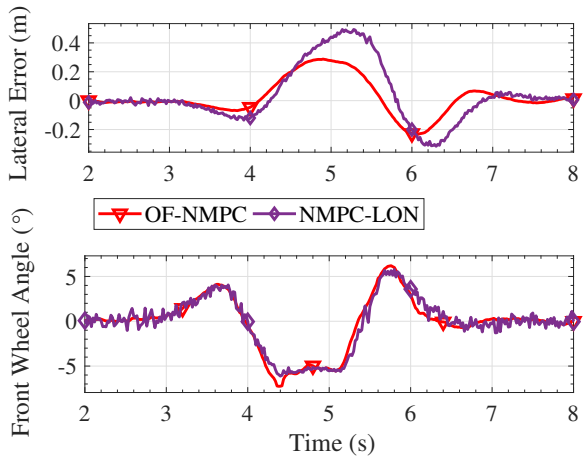

Fig. 10 Simulation results of DLC maneuver under the speed of 20m/s

In the case of the U-turn maneuver, the two controllers OF-NMPC and NMPC-LON are compared. As shown in Fig.10, the test vehicle speed is 20m/s, which is close to the stability boundary region under DLC. It can be seen from Fig.10 that NMPC-LON does not use filtered state feedback, and there are significant fluctuations in lateral position and steering wheel, while the opposite is true for OF-NMPC. This simulation

result shows that UKF successfully incorporates the vehicle dynamics model to obtain a smoother state feedback signal, which in turn results in more stable steering control. It is also effective against dynamic disturbances due to the sufficient fast filter convergence rate. In terms of lateral error, the maximum lateral error of OF-NMPC is about 28 cm, while the maximum lateral error of NMPC-LON reaches about 46 cm, which is still a significant improvement. It can be seen that OF-NMPC is still effective in improving the dynamic performance of the system.

So far, the longitudinal control performance and disturbance rejection capability have not been given sufficient attention. To verify this, the DLC maneuver with variable slope is considered.

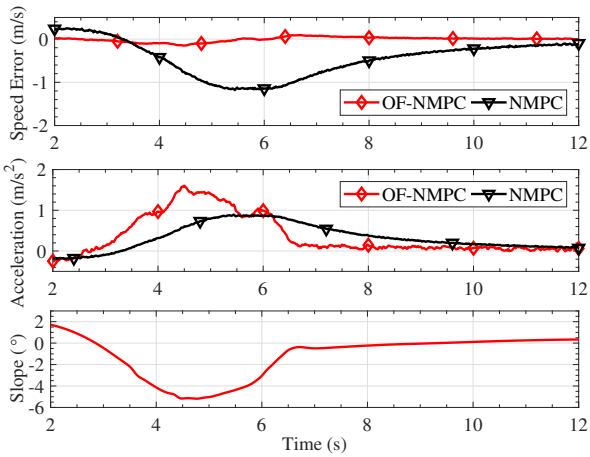

Fig. 11 Simulation results of DLC maneuver with variable slope

In order to reveal the longitudinal compensation ability for variable longitudinal disturbance, OF-NMPC and NMPC without the longitudinal and lateral disturbances compensation are compared in the variable slope condition. As shown in Fig.11, it can be seen that the slope is varying, with the maximum slope reaching 6 degrees. Since NMPC cannot compensate for longitudinal disturbances, the maximum speed error is more than 1m/s. In apparent contrast to NMPC is the speed error of OF-NMPC. The maximum error is only about 0.15m/s. The reduction in error is apparent.

It is important to note that we compensate for the longitudinal disturbances without adding any a priori information. In other words, the controller does not know the source and structure of the longitudinal disturbance. Although the varying slope disturbance is used in this simulation, any other form of longitudinal disturbance is not substantially different for the controller. Thus, the compensation effect of longitudinal disturbances applies to other forms, such as varying wind resistance.

5.4 Real vehicle experiment

Fig. 12 Aerial view real vehicle experiment

Fig.12 shows the real vehicle experiment scene. Since the main problem to be solved in this paper is the integration stability at low-speed, testing of the low-speed scene is necessary. At the same time, in order to make the test maneuver more representative, the combined maneuver is designed. As shown in Fig.13(c), the combined maneuver include DLC, straight line and S-shape maneuvers. The vehicle is tested at a speed of 1 m/s, and the controller can well maintain integration stability at such low speeds. As can be seen from Fig.13(b) and Fig.13(c), the maximum speed error is as low as 0.04m/s, and the maximum lateral error is as low as 0.04m. The controller not only ensures the stability of low-speed integration, but also ensures control accuracy.

6 Conclusions

By analyzing the stability of different explicit ODE solvers, the importance of integration stability for predictive and optimal control of nonlinear models is revealed. Qualitative and quantitative conclusions are given for the stability region of the nonlinear model predictive motion control of AVs. The stiffness of the corresponding ODE equation

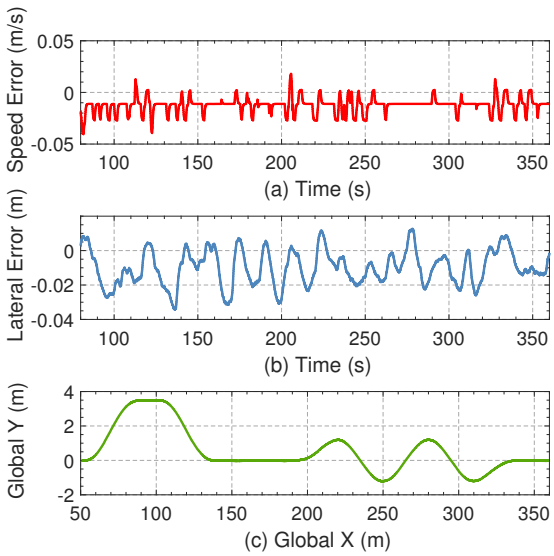

Fig. 13 Real vehicle experiment results of DLC maneuver

for the vehicle is larger at low speeds. To solve this problem, stabilized explicit ODE solvers are proposed to be applied to the motion control problem.

As a result, the proposed controller can successfully complete a U-turn maneuver with a small radius at vehicle speeds as low as 0.2m/s without using any other engineering tricks. Also due to the large increase in the stability region, larger integration steps can be used, which means fewer integration steps and fewer optimization variables. It can further improve the real-time performance of the controller. Eventually an efficient nonlinear MPC controller with a 5 ms sampling period is implemented on a micro-Autobox with a 900 MHz main frequency.

Although these findings contribute to a better understanding of the effect of integration methods and step size on nonlinear MPC control, further refinement still seems necessary. In recent years, numerous new explicit stabilized integrators have been proposed, which should be considered because of their advantages. Meanwhile the original GRAMPC is based on the gradient method, with a slow convergence rate. The accelerated gradient method will be used in future research, considering that the convergence rate is faster than the gradient method. At the same time, the computational effort is similar to the gradient method.

Acknowledgments. This work was funded by China Postdoctoral Science Foundation (Grant No. 2020M670846), Foundation of State Key Laboratory of Automotive Simulation and Control (Grant No.20180104), Science and Technology Development Plan of Jilin Province (Grant No. YDZJ202102CXJD017), and Young Elite Scientists Sponsorship Program by the China Association for Science and Technology (Grant No. YESS20200139).

Declarations

Conflict of interest: the authors declare that they have no conflict of interest.

References

[1] M. Diehl, S. Gros, Numerical optimal control. Optimization in Engineering Center (OPTEC) (2011)

[2] G. Wanner, E. Hairer, *Solving ordinary differential equations II*, vol. 375 (Springer Berlin Heidelberg, 1996)

[3] H. Peng, W. Wang, C. Xiang, L. Li, X. Wang, Torque coordinated control of four in-wheel motor independent-drive vehicles with consideration of the safety and economy. IEEE Transactions on Vehicular Technology **68**(10), 9604–9618 (2019)

[4] B. Zhao, N. Xu, H. Chen, K. Guo, Y. Huang, Design and experimental evaluations on energy-efficient control for 4wimd-evs considering tire slip energy. IEEE Transactions on Vehicular Technology (2020)

[5] C. Satzger, R. De Castro, in *2014 International Conference on Connected Vehicles and Expo (ICCVE)* (IEEE, 2014), pp. 618–624

[6] W. Xue, L. Zheng, Active collision avoidance system design based on model predictive control with varying sampling time. Automotive Innovation **3**(1), 62–72 (2020)

[7] Y. Zou, N. Guo, X. Zhang, An integrated control strategy of path following and lateral motion stabilization for autonomous distributed drive electric vehicles. Proceedings

of the Institution of Mechanical Engineers, Part D: Journal of Automobile Engineering p. 0954407019884168 (2019)

[8] M. Ataei, A. Khajepour, S. Jeon, A novel reconfigurable integrated vehicle stability control with omni actuation systems. IEEE Transactions on Vehicular Technology **67**(4), 2945–2957 (2017)

[9] M. Ataei, Reconfigurable integrated control for urban vehicles with different types of control actuation (2017)

[10] Y. Zhang, A. Khajepour, M. Ataei, A universal and reconfigurable stability control methodology for articulated vehicles with any configurations. IEEE transactions on vehicular technology **69**(4), 3748–3759 (2020)

[11] M. Ataei, A. Khajepour, S. Jeon, Model predictive control for integrated lateral stability, traction/braking control, and rollover prevention of electric vehicles. Vehicle system dynamics **58**(1), 49–73 (2020)

[12] M. Brown, J. Funke, S. Erlien, J.C. Gerdes, Safe driving envelopes for path tracking in autonomous vehicles. Control Engineering Practice **61**, 307–316 (2017)

[13] J. Ji, A. Khajepour, W.W. Melek, Y. Huang, Path planning and tracking for vehicle collision avoidance based on model predictive control with multiconstraints. IEEE Transactions on Vehicular Technology **66**(2), 952–964 (2016)

[14] E. Siampis, E. Velenis, S. Gariuolo, S. Longo, A real-time nonlinear model predictive control strategy for stabilization of an electric vehicle at the limits of handling. IEEE Transactions on Control Systems Technology **26**(6), 1982–1994 (2018). https://doi.org/10.1109/TCST.2017.2753169

[15] J.P. Allamaa, P. Listov, H. Van der Auweraer, C. Jones, T.D. Son, Real-time nonlinear mpc strategy with full vehicle validation for autonomous driving. arXiv preprint arXiv:2110.03349 (2021)

[16] A. Parra, D. Tavernini, P. Gruber, A. Sorniotti, A. Zubizarreta, J. Perez, On nonlinear model predictive control for energy-efficient torque-vectoring. IEEE Transactions on Vehicular Technology (2020)

[17] X. Liu, G. Wang, K. Chen, Nonlinear model predictive tracking control with c/gmres method for heavy-duty agvs. IEEE Transactions on Vehicular Technology **70**(12), 12,567–12,580 (2021). https://doi.org/10.1109/TVT.2021.3123176

[18] E. Kayacan, W. Saeys, H. Ramon, C. Belta, J.M. Peschel, Experimental validation of linear and nonlinear mpc on an articulated unmanned ground vehicle. IEEE/ASME Transactions on Mechatronics **23**(5), 2023–2030 (2018)

[19] G. Bai, L. Liu, Y. Meng, W. Luo, Q. Gu, B. Ma, Path tracking of mining vehicles based on nonlinear model predictive control. Applied Sciences **9**(7) (2019). https://doi.org/10.3390/app9071372. URL https://www.mdpi.com/2076-3417/9/7/1372

[20] R. Verschueren, S. De Bruyne, M. Zanon, J.V. Frasch, M. Diehl, in *53rd IEEE conference on decision and control* (IEEE, 2014), pp. 2505–2510

[21] D. Tavernini, M. Metzler, P. Gruber, A. Sorniotti, Explicit nonlinear model predictive control for electric vehicle traction control. IEEE Transactions on Control Systems Technology **27**(4), 1438–1451 (2018)

[22] M. Rokonuzzaman, N. Mohajer, S. Nahavandi, in *2019 7th International Conference on Control, Mechatronics and Automation (ICCMA)* (IEEE, 2019), pp. 266–270

[23] S. Li, S. Wang, X. Lu, S. Wang, Y. Tian, L. Guo, in *2019 Chinese Automation Congress (CAC)* (IEEE, 2019), pp. 4907–4912

[24] N. Guo, X. Zhang, Y. Zou, B. Lenzo, T. Zhang, A computationally efficient path following control strategy of autonomous

electric vehicles with yaw motion stabilization. IEEE Transactions on Transportation Electrification (2020)

[25] Y. Owaki, T. Yuno, T. Kawabe, Nonlinear model predictive control for path following of simple small electric vehicle using c/gmres. IFAC-PapersOnLine **51**(20), 253–258 (2018)

[26] P.J. van Der Houwen, B.P. Sommeijer, On the internal stability of explicit, m-stage runge-kutta methods for large m-values. ZAMM-Journal of Applied Mathematics and Mechanics/Zeitschrift für Angewandte Mathematik und Mechanik **60**(10), 479–485 (1980)

[27] B.P. Sommeijer, L.F. Shampine, J.G. Verwer, Rkc: An explicit solver for parabolic pdes. Journal of Computational and Applied Mathematics **88**(2), 315–326 (1998)

[28] A. Abdulle, A.A. Medovikov, Second order chebyshev methods based on orthogonal polynomials. Numerische Mathematik **90**(1), 1–18 (2001)

[29] A. Abdulle, Fourth order chebyshev methods with recurrence relation. SIAM Journal on Scientific Computing **23**(6), 2041–2054 (2002)

[30] A. Abdulle, Explicit stabilized runge-kutta methods. Tech. rep., Springer (2015)

[31] I. Almuslimani, G. Vilmart, Explicit stabilized integrators for stiff optimal control problems. SIAM Journal on Scientific Computing **43**(2), A721–A743 (2021)

[32] J. Martín-Vaquero, B. Kleefeld, Extrapolated stabilized explicit runge–kutta methods. Journal of Computational Physics **326**, 141–155 (2016)

[33] A. Abdulle, G. Vilmart, Pirock: A swiss-knife partitioned implicit–explicit orthogonal runge–kutta chebyshev integrator for stiff diffusion–advection–reaction problems with or without noise. Journal of Computational Physics **242**, 869–888 (2013)

[34] L. Ge, Y. Zhao, F. Ma, K. Guo, Towards longitudinal and lateral coupling control of autonomous vehicles using offset free mpc. Control Engineering Practice **121**, 105,074 (2022). https://doi.org/https://doi.org/10.1016/j.conengprac.2022.105074. URL https://www.sciencedirect.com/science/article/pii/S0967066122000065

[35] F. Borrelli, M. Morari, in *2007 46th IEEE Conference on Decision and Control* (IEEE, 2007), pp. 1245–1250

[36] G. Pannocchia, M. Gabiccini, A. Artoni, Offset-free mpc explained: novelties, subtleties, and applications. IFAC-PapersOnLine **48**(23), 342–351 (2015)

[37] G. Pannocchia, in *2015 European control conference (ECC)* (IEEE, 2015), pp. 527–532

[38] G. Betti, M. Farina, R. Scattolini, in *2012 IEEE 51st IEEE conference on decision and control (CDC)* (IEEE, 2012), pp. 5182–5187

[39] B. Käpernick, K. Graichen, in *2014 European Control Conference (ECC)* (2014), pp. 1170–1175. https://doi.org/10.1109/ECC.2014.6862353

[40] T. Englert, A. Völz, F. Mesmer, S. Rhein, K. Graichen, A software framework for embedded nonlinear model predictive control using a gradient-based augmented lagrangian approach (grampc). Optimization and Engineering **20**(3), 769–809 (2019)

[41] M. Bian, L. Chen, Y. Luo, K. Li, A dynamic model for tire/road friction estimation under combined longitudinal/lateral slip situation. Tech. rep., SAE Technical Paper (2014)

[42] W. Hirschberg, G. Rill, H. Weinfurter, Tire model tmeasy. Vehicle System Dynamics **45**(S1), 101–119 (2007)